Mathematical Modelling and Analysis
Volume 20 Number 3, May 2015, 346–368
http://dx.doi.org/10.3846/13926292.2015.1048758

Publisher: Taylor&Francis and VGTU
http://www.tandfonline.com/TMMA
ISSN: 1392-6292
eISSN: 1648-3510

A POD-Based Reduced-Order Stabilized Crank–Nicolson MFE Formulation for the Non-Stationary Parabolized Navier–Stokes Equations*

Zhendong Luo

School of Mathematics and Physics, North China Electric Power University
102206 Beijing, China
E-mail: zhdluo@ncepu.edu.cn

Received August 10, 2014; revised March 6, 2015; published online May 15, 2015

Abstract. We firstly employ a proper orthogonal decomposition (POD) method, Crank–Nicolson (CN) technique, and two local Gaussian integrals to establish a POD-based reduced-order stabilized CN mixed finite element (SCNMFE) formulation with very few degrees of freedom for non-stationary parabolized Navier–Stokes equations. Then, the error estimates of the reduced-order SCNMFE solutions, which are acted as a suggestion for choosing number of POD basis and a criterion for updating POD basis, and the algorithm implementation for the POD-based reduced-order SCNMFE formulation are provided, respectively. Finally, some numerical experiments are presented to illustrate that the numerical results are consistent with theoretical conclusions. Moreover, it is shown that the reduced-order SCNMFE formulation is feasible and efficient for finding numerical solutions of the non-stationary parabolized Navier–Stokes equations.

Keywords: proper orthogonal decomposition method, reduced-order stabilized Crank–Nicolson mixed finite element formulation, non-stationary parabolized Navier–Stokes equations, error estimate.

AMS Subject Classification: 65N12; 65M15; 65N30.

1 Introduction

For the high Reynolds number fluid flow along the x-axis direction, we may omit the second order viscous terms on the x-axis direction, but retain other second order terms and no viscous nonlinear terms. Thus, we obtain the following non-stationary parabolized Navier–Stokes equations (see [20]).

* This work was supported by National Science Foundation of China (11271127) and Science Research Project of Guizhou Province Education Department (QJHKYZ[2013]207).

Problem I. Seek $\boldsymbol{u} = (u_1, u_2)^T$ and p satisfying for $T_\infty > 0$,

$$\begin{cases} \partial_t \boldsymbol{u} + (\boldsymbol{u} \cdot \nabla)\boldsymbol{u} + \nabla p = \nu \partial_{yy}^2 \boldsymbol{u}, & (x, y, t) \in \Omega \times (0, T_\infty), \\ \operatorname{div} \boldsymbol{u} = 0, & (x, y, t) \in \Omega \times (0, T_\infty), \\ \boldsymbol{u}(x, y, t) = \boldsymbol{\varphi}(x, y, t), & (x, y, t) \in \partial\Omega \times (0, T_\infty], \\ \boldsymbol{u}(x, y, 0) = \boldsymbol{u}^0(x, y), & (x, y) \in \Omega, \end{cases} \tag{1.1}$$

where $\Omega \subset R^2$ is a bounded and connected domain, $\partial_t = \partial/\partial t$ represents the first order partial derivative with respect to time t, $\partial_{yy}^2 = \partial^2/\partial y^2$ the second order partial derivative with respect to y, $\boldsymbol{u} = (u_1, u_2)^T$ the velocity vector, p the pressure, T_∞ the total time, $\nu = (RePr)^{-1}$, Re the Reynolds number, Pr the Prandtl number, and $\boldsymbol{\varphi}(x, y, t)$ and $\boldsymbol{u}_0(x, y)$ are given vector functions. As a matter of convenience and without loss of generality, we might assume that $\boldsymbol{\varphi}(x, y, t) = \boldsymbol{0}$ in the following theoretical analysis.

A lot of numerical examples have shown that, if the fluid mainstream direction does not appear on a wide range of separation zone, the numerical results for the simplified parabolized Navier–Stokes equations are very close to those for the full Navier–Stokes equations. Especially, for fluid flow with high Reynolds number, the numerical viscosity for the full Navier–Stokes equations tends to hide some of the real physical viscosity. In other word, for fluid flow problems with high Reynolds number, the numerical solutions obtained from the parabolized Navier–Stokes equations are closer to real physical solutions than those obtained from the full Navier–Stokes equations (see [2]). Although, it seems, in principle, unreasonable that the fluid flow of the computational domain appearing separation zone is described by the simplified parabolized Navier–Stokes equations, a lot of computational examples show that, for high Reynolds number fluid flows, which feature a local small separation zone along the main stream direction (for example, the front or backward facing step flow, the separation bubble flow, the compression corner flow, the air intake channel flow field), the numerical solutions obtained by the simplified parabolized Navier–Stokes equations are very close to those obtained from the full Navier–Stokes equations (see [26]). Thus, to study the numerical methods for the non-stationary parabolized Navier–Stokes equations holds important theoretical value and real-life applied meanings.

However, most of existing numerical methods employ finite difference (FD) schemes as discrete means for the non-stationary parabolized Navier–Stokes equations (for example, see [6,26]). Unfortunately, such discretizations may result in pressure instabilities as mentioned in [4]. Thus, the finite element (FE) method for the linearized stationary parabolized equations was presented in [4]. Recently, a fully discrete stabilized Crank–Nicolson (CN) mixed FE (SCNMFE) formulation with second-order time accuracy for the non-stationary parabolized Navier–Stokes equations has been established via CN time discretization technique and two local Gaussian integrals (see [27]). It has more advantageous than the classical FE formulations in [4], for example, it can circumvent the constraint of Brezzi–Babuška (B–B) inequality in FE methods, has the second-order time accuracy, and its numerical solutions are more stable than those in [4]. And it is also different from the stabilized FE method with the

first time accuracy for the full non-stationary Navier–Stokes equations in [13]. However, it also includes a lot of degrees of freedom (i.e., unknown quantities) like other classical numerical methods if it is applied to real-life numerical simulations. Therefore, an important problem is how to reduce the degrees of freedom for the classical fully discrete SCNMFE formulation in order to alleviate the computational load, save the consuming time of calculations, and lessen the accumulation of truncation error in the computational process in a way that guarantees sufficiently accurate numerical solutions.

The proper orthogonal decomposition (POD) method (see [11]) is an effective tool for reducing the degrees of freedom in numerical models for time-dependent partial differential equations (PDEs) and to alleviate calculation load and the accumulation of truncation errors in the computational process. This method has been used to establish some POD-based reduced-order Galerkin, FE, and FD numerical models for PDEs (see [7, 9, 12, 15, 16, 17, 18]). Moreover, it has played an important role in the reduced-basis of numerical models for PDEs (see [10, 19, 21, 24, 25]).

However, to the best of our knowledge, no previous studies have used the POD method to establish POD-based reduced-order SCNMFE formulation for the non-stationary parabolized Navier–Stokes equations. Especially, most existing POD-based reduced-order models (see, e.g., [7, 9, 12, 15, 16, 18]) employ numerical solutions obtained from classical numerical models on the global time span $[0, T_\infty]$ to construct POD bases and to establish POD-based reduced-order models, before recomputing the solutions on the same time span $[0, T_\infty]$. In fact, they include repeated computations on the same time span $[0, T_\infty]$. In this study, we thoroughly improve the existing POD-based reduced-order methods, where we do only extract snapshots from the first few numerical solutions on the very short time span $[0, T_0]$ ($T_0 \ll T_\infty$) for the classical SCNMFE formulation of the non-stationary parabolized Navier–Stokes equations to formulate POD basis and establish the POD-based reduced-order SCNMFE formulation, before seeking the reduced-order SCNMFE solutions on global time span $[0, T_\infty]$. Thus, the POD-based reduced-order fully discrete SCNMFE formulation for the non-stationary parabolized Navier–Stokes equations can not only overcome those disadvantages in the existing POD-based reduced-order models (see, e.g., [7, 9, 12, 15, 16, 18]), but is also different from them.

The remainder of this paper is organized as follows. In Section 2, we recall the classical fully discrete SCNMFE formulation based on two local Gaussian integrals for the non-stationary parabolized Navier–Stokes equations. In Section 3, we employ the POD method to established the POD-based reduced-order SCNMFE formulation with very few degrees of freedom for non-stationary parabolized Navier–Stokes equations. In Section 4, we provide the error estimates of the reduced-order SCNMFE solutions, which are acted as a suggestion for choosing number of POD basis and a criterion for updating POD basis, and the algorithm implementation for the POD-based reduced-order SCNMFE formulation, respectively. In Section 5, we provide some numerical experiments to illustrate that the numerical results are consistent with theoretical conclusions. Moreover, it is shown that the reduced-order SCNMFE formulation is feasible and efficient for finding numerical solutions of the non-stationary parabolized

Navier–Stokes equations. In Section 6, we provide some main conclusions.

2 Classical Fully Discrete SCNMFE Formulation

2.1 Existence of generalized solution for Problem I

The Sobolev spaces and norms used in this article are standard (see [1]). Let $U = H_0^1(\Omega)^2$ and $M = L_0^2(\Omega) = \{q \in L^2(\Omega) : \int_\Omega q \mathrm{d}x\mathrm{d}y = 0\}$. Then the variational formulation for Problem I reads as follows.

Problem II. Seek $(\boldsymbol{u}(t), p(t)) : [0, T_\infty] \to U \times M$ satisfying

$$\begin{cases} (\boldsymbol{u}_t, \boldsymbol{v}) + a(\boldsymbol{u}, \boldsymbol{v}) + a_1(\boldsymbol{u}, \boldsymbol{u}, \boldsymbol{v}) - b(\boldsymbol{v}, p) = 0, \quad \forall \boldsymbol{v} = (v_1, v_2)^T \in U, \\ b(\boldsymbol{u}, q) = 0, \quad \forall q \in M, \\ \boldsymbol{u}(x, y, 0) = \boldsymbol{u}^0(x, y), \quad (x, y) \in \Omega, \end{cases} \tag{2.1}$$

where $a(\boldsymbol{u}, \boldsymbol{v}) = \nu(\partial_y \boldsymbol{u}, \partial_y \boldsymbol{v}) = \nu \int_\Omega (\frac{\partial u_1}{\partial y}\frac{\partial v_1}{\partial y} + \frac{\partial u_2}{\partial y}\frac{\partial v_2}{\partial y}) \mathrm{d}x\mathrm{d}y$, $b(\boldsymbol{v}, q) = (\operatorname{div} \boldsymbol{v}, q)$, $a_1(\boldsymbol{u},\ \boldsymbol{v}, \boldsymbol{w}) = [((\boldsymbol{u} \cdot \nabla)\boldsymbol{v}, \boldsymbol{w}) - ((\boldsymbol{u} \cdot \nabla)\boldsymbol{w}, \boldsymbol{v})]/2$, and $(\cdot,\cdot)$ denotes the inner product in $L^2(\Omega)$ or $L^2(\Omega)^2$.

The trilinear function $a_1(\cdot,\cdot,\cdot)$ satisfies the following properties (see [8, 13, 14, 23]):

$$\begin{aligned} &a_1(\boldsymbol{u}, \boldsymbol{v}, \boldsymbol{w}) = -a_1(\boldsymbol{u}, \boldsymbol{w}, \boldsymbol{v}), \qquad a_1(\boldsymbol{u}, \boldsymbol{v}, \boldsymbol{v}) = 0, \quad \forall \boldsymbol{u}, \boldsymbol{v}, \boldsymbol{w} \in U, \\ &\big|a_1(\boldsymbol{v}, \boldsymbol{u}, \boldsymbol{w})\big| \leqslant C \|\nabla \boldsymbol{u}\|_0 \|\nabla \boldsymbol{v}\|_0 \|\nabla \boldsymbol{w}\|_0^{\frac{1}{2}} \|\boldsymbol{w}\|_0^{\frac{1}{2}}, \quad \forall \boldsymbol{u}, \boldsymbol{v}, \boldsymbol{w} \in U, \end{aligned} \tag{2.2}$$

where $\|\boldsymbol{w}\|_0^2 = (\boldsymbol{w}, \boldsymbol{w}) = \int_\Omega |\boldsymbol{w}|^2 \mathrm{d}x\mathrm{d}y$ and C used in context is a constant which is possibly different at different occurrences.

The bilinear function $a(\cdot,\cdot)$ satisfies the following properties (see also [8, 13, 14, 23]):

$$a(\boldsymbol{v}, \boldsymbol{v}) = \nu \|\partial_y \boldsymbol{v}\|_0^2, \quad \forall \boldsymbol{v} \in U; \qquad \big|a(\boldsymbol{u}, \boldsymbol{v})\big| \leqslant \nu |\boldsymbol{u}|_1 |\boldsymbol{v}|_1, \quad \forall \boldsymbol{u}, \boldsymbol{v} \in U. \tag{2.3}$$

The bilinear function $b(\cdot,\cdot)$ satisfies the following B–B condition (see also [8, 13, 14, 23]):

$$\sup_{\boldsymbol{v} \in U} \frac{b(\boldsymbol{v}, q)}{|\boldsymbol{v}|_1} \geqslant \beta \|q\|_0, \quad \forall q \in M, \tag{2.4}$$

where β is a constant independent of $\boldsymbol{v}$ and q. Let

$$N_0 = \sup_{\boldsymbol{u}, \boldsymbol{v}, \boldsymbol{w} \in U} \frac{a_1(\boldsymbol{u}, \boldsymbol{v}, \boldsymbol{w})}{|\boldsymbol{u}|_1 \cdot |\boldsymbol{v}|_1 \cdot |\boldsymbol{w}|_1}. \tag{2.5}$$

Noting that by Poincaré inequality, there exists a constant $\bar{C}_0$ satisfying

$$\|\boldsymbol{u}\|_0 \leqslant \bar{C}_0 \|\partial_y \boldsymbol{u}\|_0, \quad \forall \boldsymbol{u} \in U. \tag{2.6}$$

The following statements of existence and stability for Problem II are provided in [27].

Theorem 1. *If* $\boldsymbol{u}^0 \in L^2(\Omega)^2$ *and* $\|\boldsymbol{u}_t(x,y,0)\|_0$ *is bounded, namely, there exists a constant* C_0 *satisfying* $\|\boldsymbol{u}_t(x,y,0)\|_0 \leqslant C_0$*, Problem II has a unique solution satisfying*

$$\|\boldsymbol{u}\|_0 + \|\boldsymbol{u}_t\|_0 + \|\partial_y \boldsymbol{u}\|_{L^2(L^2)} \leqslant C\big(\big\|\boldsymbol{u}^0\big\|_0 + \big\|\boldsymbol{u}_t(x,y,0)\big\|_0\big),$$

where $\|\cdot\|_{L^2(L^2)}$ *is the norm of* $L^2(0,T_\infty;L^2(\Omega)^2)^2$*. Further, if*

$$\|\nabla \boldsymbol{u}\|_0 \leqslant C(\|\boldsymbol{u}^0\|_0 + \|\boldsymbol{u}_t(x,y,0)\|_0),$$

then p *is also bounded, namely*

$$\|p\|_0 \leqslant C\big(\big\|\boldsymbol{u}^0\big\|_0 + \big\|\boldsymbol{u}_t(x,y,0)\big\|_0\big).$$

2.2 Time semi-discrete CN formulation for Problem I

For given positive integer N, let $k = T_\infty/N$ denote time step, $t_n = nk$, $\boldsymbol{u}^n$ is the time semi-discrete CN approximation of $\boldsymbol{u}$ at t_n $(n = 0, 1, \ldots, N)$. Let $\bar{\partial}_t \boldsymbol{u}^n = (\boldsymbol{u}^n - \boldsymbol{u}^{n-1})/k$ denote the approximation of $\boldsymbol{u}_t$, $\bar{\boldsymbol{u}}^n = (\boldsymbol{u}^n + \boldsymbol{u}^{n-1})/2$, then the time semi-discrete CN scheme with the second-order time accuracy for Problem II is described in the following.

Problem III. Seek $(\boldsymbol{u}^n, p^n) \in U \times M$ $(1 \leqslant n \leqslant N)$ satisfying

$$\begin{cases} \big(\bar{\partial}_t \boldsymbol{u}^n, \boldsymbol{v}\big) + a\big(\bar{\boldsymbol{u}}^n, \boldsymbol{v}\big) + a_1\big(\bar{\boldsymbol{u}}^n, \bar{\boldsymbol{u}}^n, \boldsymbol{v}\big) - b\big(\boldsymbol{v}, p^n\big) = 0, \quad \forall \boldsymbol{v} \in U, \\ b\big(\boldsymbol{u}^n, q\big) = 0, \quad \forall q \in M, \\ \boldsymbol{u}^0 = \boldsymbol{u}^0(x,y), \quad (x,y) \in \Omega. \end{cases}$$

The following statements of existence, stability, and convergence of solution for the time semi-discrete CN formulation, namely, Problem III are provided in [27].

Theorem 2. *If* $\boldsymbol{u}^0 \in H^1(\Omega)^2$*, then Problem III has a unique sequence of solutions* $(\boldsymbol{u}^n, p^n) \in U \times M$ $(n = 1, 2, \ldots, N)$ *that satisfy the following stability*

$$\big\|\boldsymbol{u}^n\big\|_0^2 + \frac{\nu k}{2} \sum_{i=1}^{n} \big\|\partial_y \bar{\boldsymbol{u}}^i\big\|_0^2 \leqslant \big\|\boldsymbol{u}^0\big\|_0^2, \quad n = 1, 2, \ldots, N,$$

$$\big\|\partial_y \boldsymbol{u}^n\big\|_0 \leqslant \tilde{C}_0(1 + \bar{C}_0)\big\|\partial_y \boldsymbol{u}^0\big\|_0, \quad n = 1, 2, \ldots, N,$$

where $\tilde{C}_0 = \max\{1, \sqrt{2}/(k\sqrt{\nu})\}$*. If* $\|\nabla \boldsymbol{u}^n\|_0$ *is bounded, namely there exists a constant* $\tilde{C}_1$ *satisfying* $\|\nabla \boldsymbol{u}^n\|_0 \leqslant \tilde{C}_1 \|\partial_y \boldsymbol{u}^0\|_0$*, then* p^n *is also bounded*

$$\big\|p^n\big\|_0 \leqslant \beta^{-1} k^{-1} \big[(\bar{C}_0 + \nu \bar{C}_0 + \nu)\big\|\partial_y \boldsymbol{u}^0\big\|_0 + 4^{-1} N_0 \tilde{C}_1^2 \big\|\partial_y \boldsymbol{u}^0\big\|_0^2\big].$$

Moreover, if $\boldsymbol{u} \in W^{3,\infty}(0,T;H^2(\Omega)^2)^2$ *and* $\nu^{-1}\bar{C}_0 \|\nabla \boldsymbol{u}(t)\|_{0,\infty} \leqslant 1/4$*, the following error estimates hold:*

$$\begin{aligned} &\big\|\boldsymbol{u}(t_n) - \boldsymbol{u}^n\big\|_0 + \sqrt{k}\big[\big\|\partial_y\big(\boldsymbol{u}(t_n) - \boldsymbol{u}^n\big)\big\|_0 + \big\|p(t_n) - p^n\big\|_0\big] \\ &\quad \leqslant Ck^2, \quad n = 1, 2, \ldots, N, \end{aligned}$$

where C *used subsequently is a constant which is possibly different at different occurrences, being independent of* k *and the spatial mesh size, but dependent on* $\boldsymbol{u}$*,* p*, and* ν*.*

2.3 Classical fully discrete SCNMFE formulation and the existence and the error estimates of its solutions

In the following, we are going to establish the classical fully discrete SCNMFE formulation based on two local Gaussian integrals with the second-order time accuracy directly from the time semi-discrete CN formulation. Thus, we can avoid the discussion for semi-discrete SCNFVE formulation with respect to spatial variables such that the theoretical analysis becomes simpler than the existing other methods (see, e.g., [13]).

Let $\Im_h = \{K\}$ be a quasi-uniform triangulation of Ω (see [5, 14]). FE subspaces are defined as follows.

$$U_h = \left\{ \boldsymbol{v}_h \in U \cap C(\overline{\Omega})^2 \colon \boldsymbol{v}_h|_K \in \mathcal{P}_1^2(K),\ \forall K \in \Im_h \right\},$$
$$M_h = \left\{ q_h \in M \cap C(\overline{\Omega}) \colon q_h|_K \in \mathcal{P}_1(K),\ \forall K \in \Im_h \right\},$$

where $\mathcal{P}_1$ represents the linear function space on K. It is obvious that $U_h \subset U = H_0^1(\Omega)^2$.

The following lemma is known and useful (see [14]).

Lemma 1. *Let $P_h : U \to U_h$ be a L^2-projection, i.e., for any $\boldsymbol{u} \in U$, there exists a unique $P_h\boldsymbol{u} \in U_h$ satisfying*

$$(P_h\boldsymbol{u} - \boldsymbol{u}, \boldsymbol{v}_h) = 0, \quad \forall \boldsymbol{v}_h \in U_h.$$

There hold the following error estimates

$$|P_h\boldsymbol{u} - \boldsymbol{u}|_s \leqslant Ch^{2-s}|\boldsymbol{u}|_2, \quad s = -1, 0, 1,\ \forall \boldsymbol{u} \in H^2(\Omega)^2;$$
$$\|P_h\boldsymbol{u} - \boldsymbol{u}\|_{s,\infty} \leqslant Ch^{2-s}|\boldsymbol{u}|_{2,\infty}, \quad s = 0, 1,\ \forall \boldsymbol{u} \in W^{2,\infty}(\Omega)^2.$$

Then, the classical fully discrete SCNMFE formulation based on two local Gaussian integrals with the second-order time accuracy is established as follows.

Problem IV. Seek $(\boldsymbol{u}_h^n, p_h^n) \in U_h \times M_h$ $(1 \leqslant n \leqslant N)$ satisfying

$$\begin{cases} \left(\bar{\partial}_t \boldsymbol{u}_h^n, \boldsymbol{v}_h\right) + a\left(\bar{\boldsymbol{u}}_h^n, \boldsymbol{v}_h\right) + a_1\left(\bar{\boldsymbol{u}}_h^n, \bar{\boldsymbol{u}}_h^n, \boldsymbol{v}_h\right) - b\left(\boldsymbol{v}_h, p_h^n\right) = 0, \quad \forall \boldsymbol{v}_h \in U_h, \\ b\left(\boldsymbol{u}_h^n, q_h\right) + D_h\left(p_h^n, q_h\right) = 0, \quad \forall q_h \in M_h, \\ \boldsymbol{u}_h^0 = P_h\boldsymbol{u}^0, \quad (x, y) \in \Omega, \end{cases}$$

where $D_h(p_h^n, q_h)$ is defined as follows:

$$D_h\left(p_h^n, q_h\right) = \varepsilon \sum_{K \in \Im_h} \left\{ \int_{K,2} p_h^n q_h \mathrm{d}x\mathrm{d}y - \int_{K,1} p_h^n q_h \mathrm{d}x\mathrm{d}y \right\}, \quad p_h, q_h \in M_h,$$

here ε is a positive real number, freely choosing and being independent of k and h, and $\int_{K,i} g(x, y)\mathrm{d}x\mathrm{d}y$ $(i = 1, 2)$ denote the suitable Gaussian integrals on K that is accurate for polynomials of degree i $(i = 1, 2)$ and $g(x, y) = p_h q_h$ is a polynomial whose degree is not more than i $(i = 1, 2$, see [13]).

Thus, for all test functions $q_h \in M_h$, the trial function $p_h \in M_h$ must be piecewise constant when $i = 1$. Further, we introduce the L^2-projection $\varrho_h : L^2(\Omega) \to W_h$ such that $\forall p \in L^2(\Omega)$ satisfying

$$(p, q_h) = (\varrho_h p, q_h), \quad \forall q_h \in W_h,$$

where $W_h \subset L^2(\Omega)$ is the piecewise constant subspace based on $\Im_h$. There hold the error estimates for the L^2-projection ϱ_h (see [3, 13, 14]):

$$\|\varrho_h p\|_0 \leqslant C\|p\|_0, \quad \forall p \in L^2(\Omega),$$
$$\|p - \varrho_h p\|_0 \leqslant Ch\|p\|_1, \quad \forall p \in H^1(\Omega).$$

With L^2-projection ϱ_h, the bilinear function $D_h(\cdot,\cdot)$ may be denoted by

$$D_h(p_h, q_h) = \varepsilon(p_h - \varrho_h p_h, q_h) = \varepsilon(p_h - \varrho_h p_h, q_h - \varrho_h q_h).$$

The following statements of existence, stability, and convergence of solution for Problem IV are provided in [27].

Theorem 3. *Under the hypotheses of Theorems 2, there exists a unique sequence of solutions* $(\boldsymbol{u}_h^n, p_h^n)$ $(n = 1, 2, \ldots, N)$ *to Problem IV satisfying*

$$\|\boldsymbol{u}_h^n\|_0 + \sqrt{k}\|\partial_y \boldsymbol{u}_h^n\|_0 + \sqrt{k}\|p_h^n\|_0 \leqslant C\|\boldsymbol{u}^0\|_0, \tag{2.7}$$

thereby demonstrating that the sequence of solutions of Problem IV is stable. Let $(\boldsymbol{u}, p)$ *be the solution for Problem II and* $(\boldsymbol{u}_h^n, p_h^n)$ *the solution of fully discrete SCNMFE formulation with the second-order time accuracy (that is, Problem IV). If* $h = O(k)$, $\nu^{-1}\bar{C}_0\|\nabla \bar{\boldsymbol{u}}_h^n\|_{0,\infty} \leqslant 1/4$, *and* $\boldsymbol{u}^0 \in H^2(\Omega)^2$, *there hold the following error estimates*

$$\begin{aligned}&\|\boldsymbol{u}(t_n) - \boldsymbol{u}_h^n\|_0 + \sqrt{k}\big[\|p(t_n) - p_h^n\|_0 + \|\partial_y\big(\boldsymbol{u}(t_n) - \boldsymbol{u}_h^n\big)\|_0\big]\\ &\quad \leqslant C\big(h^2 + k^2\big), \quad n = 1, 2, \ldots, N.\end{aligned}$$

Remark 1. By introducing the additional bilinear form $D_h(\cdot,\cdot)$, we stabilize the $P_1 - P_1$ FE couple such that the B–B condition is statisfied. Thus, as long as the Reynolds number Re, the Prandtl number Pr, $\boldsymbol{u}_0$, time step k, the spatial mesh size h, and finite element subspaces U_h and M_h are provided, a sequence of solutions $(\boldsymbol{u}_h^n, p_h^n) \in U_h \times M_h$ $(1 \leqslant n \leqslant N)$ is obtained by solving Problem IV. In the following section, the first L solutions $(\boldsymbol{u}_h^n, p_h^n)$ $(1 \leqslant n \leqslant L$, in general, $L \ll N$, for example, $L = 20$, but $N = 2000, 3000, 4000$, or $5000)$ are taken from N solutions $(\boldsymbol{u}_h^n, p_h^n)$ $(1 \leqslant n \leqslant N)$ as snapshots, and a POD-based reduced-order SCNMFE model is introduced.

3 Form POD Basis and Establish POD-Based Reduced-Order SCNMFE Formulation

In this section, we employ the idea mentioned in references [12,16] to formulate a POD basis (for more details, see [12, 16]) and to establish the POD-based reduced-order SCNMFE formulation for non-stationary parabolized Navier–Stokes equations.

For $(\boldsymbol{u}_h^n, p_h^n)$ $(n = 1, 2, \ldots, L)$ in Section 2, put $\boldsymbol{W}_i = (\boldsymbol{u}_h^i, p_h^i)$ $(1 \leqslant i \leqslant L)$ and $\mathcal{V} = \operatorname{span}\{\boldsymbol{W}_1, \boldsymbol{W}_2, \ldots, \boldsymbol{W}_L\}$, which is referred to as the subspace spanned by the snapshots $\{\boldsymbol{W}_i\}_{i=1}^L$, at least one of which is expected to be a non-zero vector function. Let $\{\boldsymbol{\psi}_j\}_{j=1}^l$ represent an orthonormal basis of $\mathcal{V}$ with

$l = \dim \mathcal{V}$. Then each vector of the set $\mathcal{V}$ can be denoted by

$$\boldsymbol{W}_i = \sum_{j=1}^{l} (\boldsymbol{W}_i, \boldsymbol{\psi}_j)_{U\times M} \boldsymbol{\psi}_j, \quad i = 1, 2, \ldots, L,$$

where $(\boldsymbol{W}_i, \boldsymbol{\psi}_j)_{U\times M} = (\nabla \boldsymbol{u}_h^i, \nabla \boldsymbol{\psi}_{uj}) + (p_h^i, \psi_{pj})$, $\boldsymbol{\psi}_j = (\boldsymbol{\psi}_{uj}, \psi_{pj})$, and $(\cdot,\cdot)$ is the L^2-inner product.

Definition 1. The POD method consists in seeking the orthonormal bases $\boldsymbol{\psi}_j$ $(j = 1, 2, \ldots, l)$ satisfying

$$\min_{\{\boldsymbol{\psi}_j\}_{j=1}^d} \frac{1}{L} \sum_{i=1}^{L} \left\| \boldsymbol{W}_i - \sum_{j=1}^{d} (\boldsymbol{W}_i, \boldsymbol{\psi}_j)_{U\times M} \boldsymbol{\psi}_j \right\|_{U\times M}^2 \tag{3.1}$$

subject to

$$(\boldsymbol{\psi}_r, \boldsymbol{\psi}_j)_{U\times M} = \delta_{rj}, \quad 1 \leqslant r, j \leqslant d, \tag{3.2}$$

where $\|\boldsymbol{W}_i\|_{U\times M}^2 = \|\nabla \boldsymbol{u}_h^i\|_0^2 + \|p_h^i\|_0^2$. A sequence of solutions $\{\boldsymbol{\psi}_j\}_{j=1}^d$ of (3.1)–(3.2) is referred to as a POD basis of rank d.

We formulate the correlation matrix $\boldsymbol{A} = (A_{ij})_{L\times L} \in R^{L\times L}$ associated with the snapshots $\{\boldsymbol{W}_i\}_{i=1}^L$ by

$$A_{ij} = \frac{1}{L} \left[\left(\nabla \boldsymbol{u}_h^i, \nabla \boldsymbol{u}_h^j\right) + \left(p_h^i, p_h^j\right) \right].$$

Because the matrix $\boldsymbol{A}$ with rank l is a positive semi-definite, the sequence of solutions $\{\boldsymbol{\psi}_j\}_{j=1}^d$ for (3.1)–(3.2) can be sought and there are the following conclusions (see [12, 16]).

Proposition 1. *Let $\lambda_1 \geqslant \lambda_2 \geqslant \cdots \geqslant \lambda_l > 0$ represent the positive eigenvalues of $\boldsymbol{A}$ and $\boldsymbol{v}^1, \boldsymbol{v}^2, \ldots, \boldsymbol{v}^l$ are the corresponding orthonormal eigenvectors. Then, a sequence of POD bases is obtained by*

$$\boldsymbol{\psi}_i = \frac{1}{\sqrt{L\lambda_i}} (\boldsymbol{W}_1, \boldsymbol{W}_2, \ldots, \boldsymbol{W}_L) \cdot \boldsymbol{v}^i, \quad 1 \leqslant i \leqslant d \leqslant l.$$

Moreover, we have the following error estimate

$$\frac{1}{L} \sum_{i=1}^{L} \left\| \boldsymbol{W}_i - \sum_{j=1}^{d} (\boldsymbol{W}_i, \boldsymbol{\psi}_j)_{U\times M} \boldsymbol{\psi}_j \right\|_{U\times M}^2 = \sum_{j=d+1}^{l} \lambda_j.$$

Let $U^d = \operatorname{span}\{\boldsymbol{\psi}_{u1}, \boldsymbol{\psi}_{u2}, \ldots, \boldsymbol{\psi}_{ud}\}$ and $M^d = \operatorname{span}\{\psi_{p1}, \psi_{p2}, \ldots, \psi_{pd}\}$. For $\boldsymbol{u}_h \in U_h$ and $p_h \in M_h$, a ∂_y-projection P^d: $U_h \to U^d$ about y and an L^2-projection Q^d: $M_h \to M^d$ are defined by the following formulas, respectively,

$$\begin{aligned} &\left(\partial_y P^d \boldsymbol{u}_h, \partial_y \boldsymbol{w}_d\right) = (\partial_y \boldsymbol{u}_h, \partial_y \boldsymbol{w}_d), \quad \forall \boldsymbol{w}_d \in U^d; \\ &\left(Q^d p_h, q_d\right) = (p_h, q_d), \quad \forall q_d \in M^d. \end{aligned}$$

Thus, by functional analysis theories (see, e.g., [22]), there exist two extensions P^h: $U \to U_h$ of P^d and Q^h: $M \to M_h$ of Q^d that satisfy $P^h|_{U_h} = P^d : U_h \to U^d$ and $Q^h|_{M_h} = Q^d : M_h \to M^d$, respectively, which are defined by,

$$\big(\partial_y P^h \boldsymbol{u}, \partial_y \boldsymbol{w}_h\big) = (\partial_y \boldsymbol{u}, \partial_y \boldsymbol{w}_h), \quad \forall \boldsymbol{w}_h \in U_h, \tag{3.3}$$

$$\big(Q^h p, q_h\big) = (p, q_h), \quad \forall q_h \in M_h, \tag{3.4}$$

where $(\boldsymbol{u}, p) \in U \times M$. Due to (3.3) and (3.4), the projections P^h and Q^h all are bounded

$$\big\|\partial_y\big(P^h \boldsymbol{u}\big)\big\|_0 \leqslant \big\|\partial_y \boldsymbol{u}\big\|_0, \quad \forall \boldsymbol{u} \in U; \tag{3.5}$$

$$\big\|Q^h p\big\|_0 \leqslant \|p\|_0, \quad \forall p \in M. \tag{3.6}$$

And there is the following conclusions (see [14, 16])

$$\big\|\boldsymbol{u} - P^h \boldsymbol{u}\big\|_{-1} \leqslant Ch\big\|\boldsymbol{u} - P^h \boldsymbol{u}\big\|_0 \leqslant Ch^2\big\|\partial_y\big(\boldsymbol{u} - P^h \boldsymbol{u}\big)\big\|_0, \quad \forall \boldsymbol{u} \in U.$$

Moreover, there are the following conclusions (see [14, 16]).

Lemma 2. *For every d $(1 \leqslant d \leqslant l)$, the ∂_y-projection P^d and L-projection Q^d satisfy, respectively,*

$$\frac{1}{L}\sum_{i=1}^{L}\big[\big\|\boldsymbol{u}_h^i - P^d \boldsymbol{u}_h^i\big\|_0^2 + h^2\big\|\partial_y\big(\boldsymbol{u}_h^i - P^d \boldsymbol{u}_h^i\big)\big\|_0^2\big] \leqslant Ch^2 \sum_{j=d+1}^{l} \lambda_j;$$

$$\frac{1}{L}\sum_{i=1}^{L}\big\|p_h^i - Q^d p_h^i\big\|_0^2 \leqslant \sum_{j=d+1}^{l} \lambda_j,$$

where $(\boldsymbol{u}_h^i, p_h^i) \in U_h \times M_h$ $(i = 1, 2, \ldots, L)$ are the sequence of solutions to Problem IV. Moreover, suppose that $(\boldsymbol{u}, p) \in H^2(\Omega)^2 \times H^m(\Omega)$ is the solution to Problem II, the ∂_y-projection P^h defined by (3.3)*. L^2-projection Q^h by* (3.4) *satisfy the following error estimates, respectively,*

$$\begin{aligned}&\big\|\boldsymbol{u}(t_n) - P^h \boldsymbol{u}(t_n)\big\|_{-1} + h\big\|\boldsymbol{u}(t_n) - P^h \boldsymbol{u}(t_n)\big\|_0 \\ &\qquad + h^2\big\|\partial_y(\boldsymbol{u}(t_n) - P^h \boldsymbol{u}(t_n))\big\|_0 \leqslant Ch^3, \quad n = 1, 2, \ldots, N; \\ &\big\|p(t_n) - Q^h p(t_n)\big\|_s \leqslant Ch^{m-s}, \quad n = 1, 2, \ldots, N,\ s = -1, 0,\ m = 1, 2.\end{aligned}$$

Thus, with $U^d \times M^d$, the POD-based reduced-order SCNMFE formulation for the non-stationary parabolized Navier–Stokes equations is established as follows.

Problem V. Seek $(\boldsymbol{u}_d^n, p_d^n) \in U^d \times M^d$ $(n = 1, 2, \ldots, N)$ that satisfy

$$\big(\boldsymbol{u}_d^n, p_d^n\big) = \sum_{j=1}^{d}\big(\big(\partial_y \boldsymbol{\psi}_{\boldsymbol{u}j}, \partial_y \boldsymbol{u}_h^n\big)\boldsymbol{\psi}_{\boldsymbol{u}j}, \big(\psi_{pj}, p_h^n\big)\psi_{pj}\big), \quad 0 \leqslant n \leqslant L; \tag{3.7}$$

$$\begin{aligned}&\big(\bar{\partial}_t \boldsymbol{u}_d^n, \boldsymbol{v}_d\big) + a\big(\bar{\boldsymbol{u}}_d^n, \boldsymbol{v}_d\big) + a_1\big(\bar{\boldsymbol{u}}_d^n, \bar{\boldsymbol{u}}_d^n, \boldsymbol{v}_d\big) - b\big(p_d^n, \boldsymbol{v}_d\big) = 0, \\ &\qquad \forall \boldsymbol{v}_d \in U_d,\ L+1 \leqslant n \leqslant N,\end{aligned} \tag{3.8}$$

$$b\big(\boldsymbol{u}_d^n, q_d\big) + D\big(p_d^n, q_d\big) = 0, \quad \forall q_d \in M_d,\ L+1 \leqslant n \leqslant N, \tag{3.9}$$

where $(\boldsymbol{u}_h^i, p_h^i) \in U_h \times M_h$ $(i = 1, 2, \ldots, L)$ are the first L solutions to Problem IV.

Remark 2. It is easy to see that Problem IV on each time level contains $3N_h$ degrees of freedom (where N_h is the number of vertices of triangles in $\Im_h$, see [5,14]), whereas Problem V on each time level only has $2d$ ($d \ll l \ll N \ll N_h$) degrees of freedom. For real engineering problems, the number of vertices of triangles N_h in $\Im_h$ can exceed hundreds of thousands or even one hundred million, but d is only the number of most few main eigenvalues and it is very small (for example, in Section 5, $d = 6$, while $N_h = 136 \times 10^4$). Therefore, Problem V is the POD-based reduced-order SCNMFE formulation for the nonstationary parabolized Navier–Stokes equations. Especially, Problem V only employs the first few known L solutions to Problem IV to search for other (N-L) solutions, thus providing a time extrapolation. In other words, the first L POD-based reduced-order SCNMFE solutions are obtained by projecting the first L classical SCNMFE solutions onto POD basis, while other $(N - L)$ POD-based reduced-order SCNMFE solutions are obtained by extrapolating and iterating equations (3.8) and (3.9). Therefore, it is completely different from the existing POD-based reduced-order formulations (see, e.g., [7, 9, 12, 15, 16, 18]).

4 Existence, Stability, and Convergence of Solutions and Algorithm Implementation for Problem V

4.1 Existence, stability, and convergence of solutions for the POD-based reduced-order SCNMFE formulation

In order to discuss the existence, uniqueness, stability, and convergence of the solutions for the POD-based reduced-order SCNMFE formulation Problem V, it is necessary to review the following discrete Gronwall Lemma (see [5,16]).

Lemma 3. *If $\{a_n\}$ and $\{b_n\}$ are two positive sequences, $\{c_n\}$ is a nondecreasing positive sequence, and they satisfy*

$$a_n + b_n \leqslant c_n + \bar{\lambda} \sum_{i=0}^{n-1} a_i, \quad \bar{\lambda} > 0,\ a_0 + b_0 \leqslant c_0,$$

then $a_n + b_n \leqslant c_n \exp(n\bar{\lambda})$, $n \geqslant 0$.

We have the following main conclusions for the POD-based reduced-order SCNMFE solutions.

Theorem 4. *Under the hypotheses of Theorems 2 and 3, a unique sequence of solutions $(\boldsymbol{u}_d^n, p_d^n) \in U_d \times M_d$ to Problem V exist that satisfy*

$$\|\boldsymbol{u}_d^n\|_0 + k\|\partial_y \boldsymbol{u}_d^n\|_0 + \sqrt{k}\|p_d^n\|_0 \leqslant C\|\boldsymbol{u}^0\|_0, \quad n = 1, 2, \ldots, L, L+1, \ldots, N, \tag{4.1}$$

thereby demonstrating that the sequence of solutions $(\boldsymbol{u}_d^n, p_d^n)$ $(n = 1, 2, \ldots, N)$ to Problem V is stable. If $k = O(h)$, $N = O(L^2)$, and $\bar{C}_0 \nu^{-1} \|\nabla \bar{\boldsymbol{u}}_d^n\|_{0,\infty} \leqslant 1/4$

$(n = L+1, L+2, \ldots, N)$, we have the following error estimates

$$\left\|\boldsymbol{u}_h^n - \boldsymbol{u}_d^n\right\|_0 + \sqrt{k}\left\|p_h^n - p_d^n\right\|_0 \leqslant C\left(k\sum_{j=d+1}^{l}\lambda_j\right)^{1/2}, \quad n = 1, 2, \ldots, L; \tag{4.2}$$

$$\begin{aligned}&\left\|\boldsymbol{u}_h^n - \boldsymbol{u}_d^n\right\|_0 + \sqrt{k}\left\|p_h^n - p_d^n\right\|_0 \\ &\quad\leqslant C\big(k^2+h^2\big)\sqrt{n-L} + C\left(k\sum_{j=d+1}^{l}\lambda_j\right)^{1/2}, \quad n = L+1, L+2, \ldots, N.\end{aligned} \tag{4.3}$$

Proof. If $1 \leqslant n \leqslant L$, from (3.7), we obtain a unique sequence of solutions $(\boldsymbol{u}_d^n, p_d^n) \in U^d \times M^d$ $(n = 1, 2, \ldots, L)$ to Problem V. Because finite dimensional subspaces $U^d \times M^d$ are sequentially compact Hilbert spaces, if (4.1) holds when $L+1 \leqslant n \leqslant N$, applying fixed point theorem (see [22]) to (3.8)–(3.9), we obtain a unique sequence of solutions $(\boldsymbol{u}_d^n, p_d^n) \in U^d \times M^d$ $(n = L+1, L+2, \ldots, N)$ to Problem V. Thus, there exists a unique sequence of solutions $(\boldsymbol{u}_d^n, p_d^n) \in U^d \times M^d$ $(n = 1, 2, \ldots, N)$ to Problem V. Therefore, we first devote to proving that (4.1) holds.

If $n = 1, 2, \ldots, L$, the inequality (4.1) in Theorem 4 are easily obtained by Theorem 3, (3.5), and (3.6). If $n = L+1, L+2, \ldots, N$, by taking $\boldsymbol{v}_d = \bar{\boldsymbol{u}}_d^n$ in the second equation of Problem V and $q_d = p_d^n$ in the third equation of Problem V and by using Lemma 2 and the Hölder and Cauchy inequalities, we obtain

$$\begin{aligned}&\frac{1}{2}\big(\left\|\boldsymbol{u}_d^n\right\|_0^2 - \left\|\boldsymbol{u}_d^{n-1}\right\|_0^2\big) + k\nu\left\|\partial_y\bar{\boldsymbol{u}}_d^n\right\|_0^2 + k\varepsilon\left\|p_d^n - \varrho_h p_d^n\right\|_0^2 \\ &\quad= k\varepsilon\big(p_d^{n-1} - \varrho_h p_d^{n-1}, p_d^n - \varrho_h p_d^n\big) \\ &\quad\leqslant \frac{k\varepsilon}{2}\left\|p_d^n - \varrho_h p_d^n\right\|_0^2 + \frac{k\varepsilon}{2}\left\|p_d^{n-1} - \varrho_h p_d^{n-1}\right\|_0^2.\end{aligned} \tag{4.4}$$

It follows from (4.4) that

$$\begin{aligned}&\left\|\boldsymbol{u}_d^n\right\|_0^2 - \left\|\boldsymbol{u}_d^{n-1}\right\|_0^2 + 2k\nu\left\|\partial_y\bar{\boldsymbol{u}}_d^n\right\|_0^2 + k\varepsilon\left\|p_d^n - \varrho_h p_d^n\right\|_0^2 \\ &\quad\leqslant k\varepsilon\left\|p_d^{n-1} - \varrho_h p_d^{n-1}\right\|_0^2.\end{aligned} \tag{4.5}$$

Summing (4.5) from $L+1$ to n and using the case of (4.1) when $n = 1, 2, \ldots, L$ yield

$$\begin{aligned}&\left\|\boldsymbol{u}_d^n\right\|_0^2 + k\nu\sum_{i=L+1}^{n}\left\|\partial_y\bar{\boldsymbol{u}}_d^i\right\|_0^2 + k\varepsilon\left\|p_d^n - \varrho_h p_d^n\right\|_0^2 \\ &\quad\leqslant \left\|\boldsymbol{u}_d^n\right\|_0^2 + 2k\nu\sum_{i=L+1}^{n}\left\|\partial_y\bar{\boldsymbol{u}}_d^i\right\|_0^2 + k\varepsilon\left\|p_d^n - \varrho_h p_d^n\right\|_0^2 \leqslant C\left\|\boldsymbol{u}_d^0\right\|_0^2.\end{aligned} \tag{4.6}$$

Noting that $\sum_{i=1}^{n} a_i^2 \geqslant \left(\sum_{i=1}^{n} a_i\right)^2/n$ and $\|a+b\|_0 \geqslant \|a\|_0 - \|b\|_0$, from (4.6), we obtain

$$\left\|\boldsymbol{u}_d^n\right\|_0 + k\sqrt{\nu}\left\|\partial_y\boldsymbol{u}_d^n\right\|_0 + \sqrt{k\varepsilon}\big(\left\|p_d^n\right\|_0 - \left\|\varrho_h p_d^n\right\|_0\big) \leqslant C\left\|\boldsymbol{u}_d^0\right\|_0. \tag{4.7}$$

If $p_d^n \neq 0$, then $\|p_d^n\|_0 > \|\varrho_h p_d^n\|_0$. Thus, there is a constant $\alpha \in (0.1)$ satisfying $\alpha\|p_d^n\|_0 = \|\varrho_h p_d^n\|_0$. Therefore, from (4.7), we obtain (4.1) when $n = L+1, L+2, \ldots, N$. If $p_d^n = 0$, (4.1) is obviously correct.

If $n = 1, 2, \ldots, L$, from Lemma 2, we can obtain (4.2). If $n = L+1, L+2, \ldots, N$, by noting that $U_d \subset U_h$ and $M_d \subset M_h$ and subtracting Problem V from Problem IV taking $\boldsymbol{v}_h = \boldsymbol{v}_d$ and $q_h = q_d$, we obtain the following system of error equations:

$$\begin{cases} \big(\boldsymbol{u}_h^n - \boldsymbol{u}_d^n, \boldsymbol{v}_d\big) + ka\big(\bar{\boldsymbol{u}}_h^n - \bar{\boldsymbol{u}}_d^n, \boldsymbol{v}_d\big) + ka_1\big(\bar{\boldsymbol{u}}_h^n, \bar{\boldsymbol{u}}_h^n, \boldsymbol{v}_d\big) \\ \qquad - ka_1\big(\bar{\boldsymbol{u}}_d^n, \bar{\boldsymbol{u}}_d^n, \boldsymbol{v}_d\big) - kb\big(\boldsymbol{v}_d, p_h^n - p_d^n\big) \\ \quad = \big(\boldsymbol{u}_h^{n-1} - \boldsymbol{u}_d^{n-1}, \boldsymbol{v}_d\big), \quad \forall \boldsymbol{v}_d \in U_d,\ n = L+1, L+2, \ldots, N; \\ b\big(\boldsymbol{u}_h^n - \boldsymbol{u}_d^n, q_d\big) + D\big(p_h^n - p_d^n, q_d\big) = 0, \quad \forall q_d \in M_d. \end{cases} \tag{4.8}$$

Put $\boldsymbol{e}^n = P^d\boldsymbol{u}_h^n - \boldsymbol{u}_d^n$, $\boldsymbol{\rho}^n = \boldsymbol{u}_h^n - P^d\boldsymbol{u}_h^n$, $\eta^n = Q^d p_h^n - p_d^n$, and $\xi^n = p_h^n - Q^d p_h^n$. Thus, on the one hand, it is obtained by using Lemma 2, the system of error equations (4.8), and the properties of operator ϱ_h that

$$\begin{aligned} &2\big(\|\boldsymbol{e}^n\|_0^2 - \|\boldsymbol{e}^{n-1}\|_0^2\big) + k\nu\big\|\partial_y\big(\boldsymbol{e}^n + \boldsymbol{e}^{n-1}\big)\big\|_0^2 \\ &\quad = 2\big(\boldsymbol{\rho}^{n-1} - \boldsymbol{\rho}^n, \boldsymbol{e}^n + \boldsymbol{e}^{n-1}\big) + 2ka\big(\bar{\boldsymbol{u}}_h^n - \bar{\boldsymbol{u}}_d^n, \boldsymbol{e}^n + \boldsymbol{e}^{n-1}\big) \\ &\qquad + 2\big(\boldsymbol{u}_h^n - \boldsymbol{u}_d^n - \big(\boldsymbol{u}_h^{n-1} - \boldsymbol{u}_d^{n-1}\big), \boldsymbol{e}^n + \boldsymbol{e}^{n-1}\big) \\ &\qquad - 2ka\big(\boldsymbol{\rho}^n + \boldsymbol{\rho}^{n-1}, \boldsymbol{e}^n + \boldsymbol{e}^{n-1}\big) \\ &\quad = 2\big(\boldsymbol{\rho}^{n-1} - \boldsymbol{\rho}^n, \boldsymbol{e}^n + \boldsymbol{e}^{n-1}\big) + 2kb\big(\boldsymbol{e}^n + \boldsymbol{e}^{n-1}, p_h^n - p_d^n\big) \\ &\qquad - 2\big(\boldsymbol{u}_h^{n-1} - \boldsymbol{u}_d^{n-1}, \boldsymbol{e}^n + \boldsymbol{e}^{n-1}\big) \\ &\qquad - ka_1\big(\bar{\boldsymbol{u}}_h^n, \bar{\boldsymbol{u}}_h^n, \boldsymbol{e}^n + \boldsymbol{e}^{n-1}\big) + ka_1\big(\bar{\boldsymbol{u}}_d^n, \bar{\boldsymbol{u}}_d^n, \boldsymbol{e}^n + \boldsymbol{e}^{n-1}\big) \\ &\quad = 2\big(\boldsymbol{\rho}^{n-1} - \boldsymbol{\rho}^n, \boldsymbol{e}^n + \boldsymbol{e}^{n-1}\big) + 2kb\big(\xi^n, \boldsymbol{e}^n + \boldsymbol{e}^{n-1}\big) \\ &\qquad - 2\big(\boldsymbol{u}_h^{n-1} - \boldsymbol{u}_d^{n-1}, \boldsymbol{e}^n + \boldsymbol{e}^{n-1}\big) \\ &\qquad - 2k\big(p_h^n + p_h^{n-1} - p_d^n - p_d^{n-1} - \varrho_h\big(p_h^n + p_h^{n-1} - p_d^n - p_d^{n-1}\big), \eta^n\big) \\ &\qquad - ka_1\big(\bar{\boldsymbol{u}}_h^n, \bar{\boldsymbol{u}}_h^n, \boldsymbol{e}^n + \boldsymbol{e}^{n-1}\big) + ka_1\big(\bar{\boldsymbol{u}}_d^n, \bar{\boldsymbol{u}}_d^n, \boldsymbol{e}^n + \boldsymbol{e}^{n-1}\big) \\ &\quad \leqslant C\big(k^{-1}\|\boldsymbol{\rho}^{n-1} - \boldsymbol{\rho}^n\|_{-1}^2 + k\|\boldsymbol{\rho}^{n-1}\|_0^2 + \|\boldsymbol{e}^{n-1}\|_0^2\big) + Ck\|\xi^n\|_0^2 \\ &\qquad - 2k\big(p_h^n + p_h^{n-1} - p_d^n - p_d^{n-1} - \varrho_h\big(p_h^n + p_h^{n-1} - p_d^n - p_d^{n-1}\big), \eta^n\big). \\ &\qquad + \frac{k\nu}{4}\big\|\nabla\big(\boldsymbol{e}^n + \boldsymbol{e}^{n-1}\big)\big\|_0^2 - ka_1\big(\bar{\boldsymbol{u}}_h^n, \bar{\boldsymbol{u}}_h^n, \boldsymbol{e}^n + \boldsymbol{e}^{n-1}\big) \\ &\qquad + ka_1\big(\bar{\boldsymbol{u}}_d^n, \bar{\boldsymbol{u}}_d^n, \boldsymbol{e}^n + \boldsymbol{e}^{n-1}\big). \end{aligned} \tag{4.9}$$

Next, by triangle inequality, we have

$$\begin{aligned} &- 2k\big(p_h^n + p_h^{n-1} - p_d^n - p_d^{n-1} - \varrho_h\big(p_h^n + p_h^{n-1} - p_d^n - p_d^{n-1}\big), \eta^n\big) \\ &\quad = -2k\big(\eta^n - \varrho_h\eta^n, \eta^n - \varrho_h\eta^n\big) - 2k\big(\eta^{n-1} - \varrho_h\eta^{n-1}, \eta^n - \varrho_h\eta^n\big) \\ &\quad \leqslant -2k\big(\|\eta^n\|_0^2 - \|\varrho_h\eta^n\|_0^2\big) + k\big(\|\eta^{n-1}\|_0^2 - \|\varrho_h\eta^{n-1}\|_0^2\big) \\ &\qquad + k\big(\|\eta^n\|_0^2 - \|\varrho_h\eta^n\|_0^2\big) \\ &\quad \leqslant k\big(\|\eta^{n-1}\|_0^2 - \|\varrho_h\eta^{n-1}\|_0^2\big) - k\big(\|\eta^n\|_0^2 - \|\varrho_h\eta^n\|_0^2\big). \end{aligned} \tag{4.10}$$

In addition, if $\bar{C}_0\nu^{-1}\|\nabla\bar{\boldsymbol{u}}_h^n\|_{0,\infty}\leqslant 1/4$ and $\bar{C}_0\nu^{-1}\|\nabla\bar{\boldsymbol{u}}_d^n\|_{0,\infty}\leqslant 1/4$ ($n=L+1$, $L+2,\ldots,N$), by the properties of $a_1(.,.,.)$, (2.6), and Lemma 2, we have

$$\begin{aligned}&ka_1\big(\bar{\boldsymbol{u}}_d^n,\bar{\boldsymbol{u}}_d^n,\boldsymbol{e}^n+\boldsymbol{e}^{n-1}\big)-ka_1\big(\bar{\boldsymbol{u}}_h^n,\bar{\boldsymbol{u}}_h^n,\boldsymbol{e}^n+\boldsymbol{e}^{n-1}\big)\\&\quad\leqslant Ck\|\boldsymbol{\rho}\|_0^2+\frac{k\nu}{4}\big\|\partial_y\big(\boldsymbol{e}^n+\boldsymbol{e}^{n-1}\big)\big\|_0^2.\end{aligned}\tag{4.11}$$

Thus, if $k=O(h)$, combining (4.10) and (4.11) with (4.9) yields that

$$\begin{aligned}&4\big(\big\|\boldsymbol{e}^n\big\|_0^2-\big\|\boldsymbol{e}^{n-1}\big\|_0^2\big)+k\nu\big\|\partial_y\big(\boldsymbol{e}^n+\boldsymbol{e}^{n-1}\big)\big\|_0^2+4k\big(\big\|\eta^n\big\|_0^2-\big\|\varrho_h\eta^n\big\|_0^2\big)\\&\quad\leqslant C\big(k\big\|\boldsymbol{\rho}^n\big\|_0^2+k\big\|\boldsymbol{\rho}^{n-1}\big\|_0^2+\big\|\boldsymbol{e}^{n-1}\big\|_0^2\big)+Ck\big\|\xi^n\big\|_0^2\\&\qquad+4k\big(\big\|\eta^{n-1}\big\|_0^2-\big\|\varrho_h\eta^{n-1}\big\|_0^2\big).\end{aligned}\tag{4.12}$$

Summing (4.12) from $L+1$ to n and using Lemma 2 yield that

$$\begin{aligned}&4\big\|\boldsymbol{e}^n\big\|_0^2+k\mu\sum_{i=L+1}^{n}\big\|\partial_y(\boldsymbol{e}^i+\boldsymbol{e}^{i-1})\big\|_0^2+2k\big(\big\|\eta^n\big\|_0^2-\big\|\varrho_h\eta^n\big\|_0^2\big)\\&\quad\leqslant 4\big\|\boldsymbol{e}^L\big\|_0^2+4k\big(\big\|\eta^L\big\|_0^2-\big\|\varrho_h\eta^L\big\|_0^2\big)\\&\qquad+Ck\left[\sum_{i=L}^{n}\big(\big\|\boldsymbol{\rho}^i\big\|_0^2+\big\|\xi^i\big\|_0^2\big)+\sum_{i=L}^{n-1}\big\|\boldsymbol{e}^i\big\|_0^2\right].\end{aligned}\tag{4.13}$$

If $\eta^n\neq 0$, there hold $\|\eta^n\|_0^2>\|\varrho_h\eta^n\|_0^2$ ($n=L,L+1,\ldots,N$). Thus, there are $\alpha_1\in(0,1)$ and $\alpha_2\in(0,1)$ that satisfy $\alpha_1\|\eta^n\|_0^2=\|\varrho_h\eta^n\|_0^2$ and $\alpha_2\|\eta^L\|_0^2=\|\varrho_h\eta^L\|_0^2$. Then, we could simplify (4.13) into the following inequality

$$\begin{aligned}&\big\|\boldsymbol{e}^n\big\|_0^2+k\sum_{i=L+1}^{n}\big\|\partial_y\big(\boldsymbol{e}^i+\boldsymbol{e}^{i-1}\big)\big\|_0^2+k\big\|\eta^n\big\|_0^2\\&\quad\leqslant C\big\|\boldsymbol{e}^L\big\|_0^2+Ck\big\|\eta^L\big\|_0^2+Ck\left[\sum_{i=L}^{n}\big(\big\|\boldsymbol{\rho}^i\big\|_0^2+\big\|\xi^i\big\|_0^2\big)+\sum_{i=L}^{n-1}\big\|\boldsymbol{e}^i\big\|_0^2\right].\end{aligned}\tag{4.14}$$

Applying Lemma 3 to (4.14) yields

$$\begin{aligned}&\big\|\boldsymbol{e}^n\big\|_0^2+k\sum_{i=L+1}^{n}\big\|\partial_y\big(\boldsymbol{e}^i+\boldsymbol{e}^{i-1}\big)\big\|_0^2+k\big\|\eta^n\big\|_0^2\\&\quad\leqslant C\left[\big\|\boldsymbol{e}^L\big\|_0^2+k\big\|\eta^L\big\|_0^2+k\sum_{i=L}^{n}\big(\big\|\boldsymbol{\rho}^i\big\|_0^2+\big\|\xi^i\big\|_0^2\big)\right]\exp\big(C(n-L)k\big).\end{aligned}\tag{4.15}$$

By extracting the square root for (4.15) and using $(\sum_{i=1}^n b_i^2)^{1/2}\geqslant\sum_{i=1}^n|b_i|/\sqrt{n}$ and $\|\partial_y(\boldsymbol{e}^n+\boldsymbol{e}^{n-1})\|_0\geqslant\|\partial_y\boldsymbol{e}^n\|_0-\|\partial_y\boldsymbol{e}^{n-1}\|_0$, we obtain

$$\begin{aligned}&\big\|\boldsymbol{e}^n\big\|_0+k\big\|\partial_y\boldsymbol{e}^n\big\|_0+k^{1/2}\big\|\eta^n\big\|_0\\&\quad\leqslant C\left[\big\|\boldsymbol{e}^L\big\|_0^2+k\big\|\eta^L\big\|_0^2+k\sum_{i=L}^{n}\big(\big\|\boldsymbol{\rho}^i\big\|_0^2+\big\|\xi^i\big\|_0^2\big)\right]^{1/2}.\end{aligned}\tag{4.16}$$

Moreover, from Lemma 2 and Theorem 3, we obtain

$$\begin{aligned}\left\|\boldsymbol{\rho}^i\right\|_0 &\leqslant \left\|\boldsymbol{u}_h^i - \boldsymbol{u}(t_i)\right\|_0 + \left\|\boldsymbol{u}(t_i) - P^h\boldsymbol{u}(t_i)\right\|_0 + \left\|P^h\big(\boldsymbol{u}(t_i) - \boldsymbol{u}_h^i\big)\right\|_0 \\ &\leqslant C\big[\left\|\boldsymbol{u}(t_i) - P^h\boldsymbol{u}(t_i)\right\|_0 + \left\|\boldsymbol{u}(t_i) - \boldsymbol{u}_h^i\right\|_0\big] \leqslant C\big(h^2 + k^2\big), \qquad (4.17)\end{aligned}$$

$$\begin{aligned}k\left\|p_h^i - Q^d p_h^i\right\|_0 &\leqslant k\big[\left\|p_h^i - p(t_i)\right\|_0 + \left\|p(t_i) - Q^h p(t_i)\right\|_0 + \left\|Q^h\big(p(t_i) - p_h^i\big)\right\|_0\big] \\ &\leqslant Ck\big[\left\|p(t_i) - Q^h p(t_i)\right\|_0 + \left\|p(t_i) - p_h^i\right\|_0\big] \leqslant C\big(h^2 + k^2\big). \qquad (4.18)\end{aligned}$$

Combining (4.17) and (4.18) with (4.16) and using Lemma 2 and (4.2) yield (4.3). If $\eta^n = 0$, the error estimates (4.3) is obviously correct, which completes the proof of Theorem 4. □

Combining Theorem 4 and Theorem 3 yields the following result.

Theorem 5. *Under the hypotheses of Theorems 4, the error estimates between the solution* $(\boldsymbol{u}, p)$ *to Problem* II *and the solutions* $(\boldsymbol{u}_d^n, p_d^n)$ *to Problem V hold, as follows*

$$\begin{aligned}&\left\|\boldsymbol{u}(t_n) - \boldsymbol{u}_d^n\right\|_0 + \sqrt{k}\left\|p(t_n) - p_d^n\right\|_0 \\ &\quad\leqslant \tilde{M}(n) + C\big(k^2 + h^2\big) + C\left(k\sum_{j=d+1}^{l}\lambda_j\right)^{1/2}, \quad 1 \leqslant n \leqslant N,\end{aligned}$$

where $\tilde{M}(n) = 0$ $(1 \leqslant n \leqslant L)$, *but* $\tilde{M}(n) = C(k^2+h^2)\sqrt{n-L}$ $(L+1 \leqslant n \leqslant N)$.

Remark 3. From (2.7) in Theorem 3 and (4.1) in Theorem 4 as well as their proofs, it is easily seen that the conditions $\bar{C}_0\nu^{-1}\|\nabla\bar{\boldsymbol{u}}_h^n\|_{0,\infty} \leqslant 1/4$ and $\bar{C}_0\nu^{-1}\|\nabla\bar{\boldsymbol{u}}_d^n\|_{0,\infty} \leqslant 1/4$ $(n = L+1, L+2, \ldots, N)$ hold if only $\|\boldsymbol{u}^0\|_0$ is sufficiently small. The term $(k\sum_{j=d+1}^{l}\lambda_j)^{1/2}$ in Theorems 4 and 5 is caused by POD-based reduced-order and the terms $(k^2+h^2)\sqrt{n-L}$ $(L+1 \leqslant n \leqslant N)$ are caused by extrapolation and iteration, i.e., the errors of the the POD-based reduced-order SCNMFE solutions are more terms $(k\sum_{j=d+1}^{l}\lambda_j)^{1/2}$ and $(k^2+h^2)\sqrt{n-L}$ $(L+1 \leqslant n \leqslant N)$ than those of the classical SCNMFE solutions, but the degrees of freedom for the POD-based reduced-order SCNMFE formulation Problem V are far less than those for the classical SCNMFE formulation Problem IV so that Problem V can greatly lessen the truncation error accumulation in the computational process, alleviate the calculating load, save the consuming time of calculations, and improve actual computational accuracy (see the examples in Section 5). Moreover, the errors $(k\sum_{j=d+1}^{l}\lambda_j)^{1/2}$ could be used as a suggestion to choose the number of POD basis, that is, it is necessary to take d satisfying $k\sum_{j=d+1}^{l}\lambda_j = O(k^4, h^4)$, while the terms $(k^2+h^2)\sqrt{n-L}$ $(L+1 \leqslant n \leqslant N)$ can be used to guide the POD update.

4.2 Algorithm implementation for the POD-based reduced-order SCNMFE formulation

It is possible to solve the POD-based reduced-order SCNMFE formulation Problem V by the following seven steps.

Step 1. Extract the snapshots $\boldsymbol{W}_i(x,y) = (\boldsymbol{u}_h^i, p_h^i)$ $(i = 1, 2, \ldots, L \ll N)$ from the classical SCNMVE solutions to Problem IV or the samples drawing from actual physical system trajectories.
Step 2. Form the correlation matrix $\boldsymbol{A} = (A_{ij})_{L\times L}$, where $A_{ij} = [(\nabla \boldsymbol{u}_h^i, \nabla \boldsymbol{u}_h^j) + (p_h^i, p_h^j)]/L$.
Step 3. Let $\boldsymbol{v} = (a_1, a_2, \ldots, a_L)^T$. Solve the eigenvalue equation $\boldsymbol{A}\boldsymbol{v} = \lambda \boldsymbol{v}$ to obtain eigenvalues $\lambda_1 \geqslant \lambda_2 \geqslant \cdots \geqslant \lambda_l > 0$ $(l = \dim\{\boldsymbol{W}_1, \boldsymbol{W}_2, \ldots, \boldsymbol{W}_L\})$ and their associated eigenvectors $\boldsymbol{v}^j = (a_1^j, a_2^j, \ldots, a_L^j)^T$ $(k = 1, 2, \ldots, l)$.
Step 4. For given spatial grid diameter h and time step k, and the required error δ, determine the number d of the POD basis to satisfy $k^4 + h^4 + k\sum_{j=d+1}^{l} \lambda_j \leqslant \delta^2$.
Step 5. Formulate POD basis

$$(\boldsymbol{\psi}_{uj}(x,y), \psi_{pj}(x,y)) = \sum_{i=1}^{L} a_i^j \left(\boldsymbol{u}_h^i, p_h^i\right) / \sqrt{L\lambda_j}, \quad j = 1, 2, \ldots, d.$$

Step 6. Take $U^d = \text{span}\{\boldsymbol{\psi}_{u1}(x,y), \boldsymbol{\psi}_{u2}(x,y), \ldots, \boldsymbol{\psi}_{ud}(x,y)\}$ and $M^d = \text{span}\{\psi_{p1}(x,y), \psi_{p2}(x,y), \ldots, \psi_{pd}(x,y)\}$ and solve Problem V to obtain the the POD-based reduced-order SCNMFE solutions $(\boldsymbol{u}_d^n, p_d^n)$ $(n = 1, 2, \ldots, L, L+1, \ldots, N)$.
Step 7. If $(k^2 + h^2)\sqrt{n - L} \leqslant \delta$, then $(\boldsymbol{u}_d^n, p_d^n)$ $(n = 1, 2, \ldots, N)$ are the solutions to the POD-based reduced-order SCNMFE formulation that satisfy the accuracy requirement. Else, i.e., if $(k^2 + h^2)\sqrt{n - L} > \delta$, let $(\boldsymbol{u}_h^i, p_h^i) = (\boldsymbol{u}_d^i, p_d^i)$ $(i = n - L, n - L - 1, \ldots, n - 1)$, return Step 2.

Remark 4. Step 7 could be changed into that if $\|\boldsymbol{u}_d^{n-1} - \boldsymbol{u}_d^n\|_0 \geqslant \|\boldsymbol{u}_d^n - \boldsymbol{u}_d^{n+1}\|_0$ and $\|p_d^{n-1} - p_d^n\|_0 \geqslant \|p_d^n - p_d^{n+1}\|_0$ $(n = L, L+1, \ldots, N-1)$, then $(\boldsymbol{u}_d^n, p_d^n)$ $(n = 1, 2, \ldots, N)$ are the solutions to the POD-based reduced-order SCNMFE formulation that satisfy accuracy requirement. Else, i.e., if $\|\boldsymbol{u}_d^{n-1} - \boldsymbol{u}_d^n\|_0 < \|\boldsymbol{u}_d^n - \boldsymbol{u}_d^{n+1}\|_0$ or $\|p_d^{n-1} - p_d^n\|_0 < \|p_d^n - p_d^{n+1}\|_0$ $(n = L, L+1, \ldots, N-1)$, let $(\boldsymbol{u}_h^i, p_h^i) = (\boldsymbol{u}_d^i, p_d^i)$ $(i = n - L, n - L - 1, \ldots, n - 1)$, return Step 2.

5 Some Numerical Experiments

In this section, some numerical experiments are used to demonstrate the feasibility and efficiency of the POD-based reduced-order SCNMFE formulation for the non-stationary parabolized Navier–Stokes equations, which validate that the numerical results are consistent with theoretical conclusions.

The computational domain Ω comprises a channel with a width of 6 and a length of 20, with two identical rectangular cavities a the bottom and the top of the channel. Two rectangular cavities both have a width of 2 and a length of 4 (see Figure 1). A structured mesh with side length $\triangle x = \triangle y = 0.01$ is employed. And then each square is linked with diagonal in the same direction divided into two triangles, which constitutes triangularizations $\Im_h$ with $h = \sqrt{2} \times 10^{-2}$. Take $Re = 1000$, $Pr = 7$, and $\varepsilon = 1$. Except for the inflow of the left boundary with a velocity of $\boldsymbol{u} = (0.1(y-2)(8-y), 0)^T$ $(x = 0, 2 \leqslant y \leqslant 8)$ and the outflow of the right boundary with velocity of $\boldsymbol{u} = (u_1, u_2)^T$ satisfying

$u_2 = 0$ and $u_1(x, y, t) = u_1(19, y, t)$ $(19 \leqslant x \leqslant 20, 2 \leqslant y \leqslant 8, 0 \leqslant t \leqslant T_\infty)$, all of the initial and boundary value conditions are taken as $\mathbf{0}$. In order to satisfy $k = O(h)$, the time step increment is taken as $k = 0.01$.

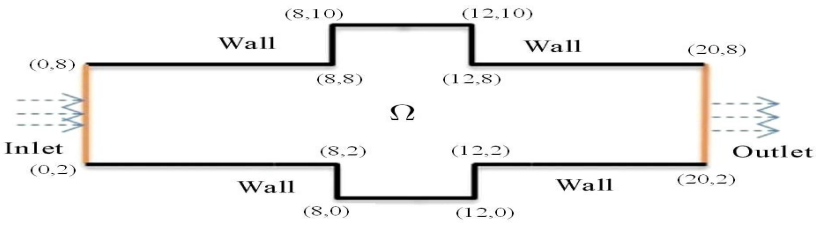

Figure 1. The computational field and boundary conditions of flow.

First, 20 numerical solutions $(\boldsymbol{u}_h^n, p_h^n)$ $(n = 1, 2, \ldots, 20)$ obtained from the classical SCNMFE formulation Problem IV are used to form snapshots $\boldsymbol{W}_i = (\boldsymbol{u}_h^i, p_h^i)$ $(i = 1, 2, \ldots, 20)$. And then, 20 eigenvalues which are arranged in a decreasing order, and their associated 20 eigenvectors were found by using Step 3 in Section 4.2. This was achieved by computing that error factor $(k \sum_{j=7}^{20} \lambda_j)^{1/2} \leqslant 6.5 \times 10^{-4}$ when $k = 0.01$ and $L = 20$. Thus, it was only necessary to take the main six eigenvectors $(\boldsymbol{\psi}_{uj}, \psi_{pj})$ $(j = 1, 2, \ldots, 6)$ to expand into subspaces $U^d \times M^d$, before finding the numerical solutions $(\boldsymbol{u}_d^n, p_d^n)$ $(n = 2000,\ 3000,\ 4000,$ and $5000,$ that is, at $t = 2,\ 3,\ 4,$ and $5)$ using the POD-based reduced-order SCNMFE formulation according to the seven steps in Section 4.2, for which the velocity and pressure numerical solutions are depicted graphically in the bottom charts shown in Figures 2 and 3 (at $t = 2$), 4 and 5 (at $t = 3$), 6 and 7 (at $t = 4$), 8 and 9 (at $t = 5$). The numerical solutions of the velocity and pressure obtained by the classical SCNMFE formulation of Problem IV are depicted graphically in the top charts in Figures 2 and 3 (at $t = 2$), 4 and 5 (at $t = 3$), 6 and 7 (at $t = 4$), 8 and 9 (at $t = 5$), respectively.

Each of the two charts from Figure 2 to Figure 8 exhibits quasi-identical similarity. The errors of the POD-based reduced-order SCNMFE solutions on the starting time-span are slightly larger than those of classical SCNMFE solutions, but since the POD-based reduced-order SCNMFE formulation on each time-level only had 2×6 degrees of freedom whereas the classical SCNMFE formulation on each time-level had $3 \times 136 \times 10^4$ degrees of freedom, i.e., the degrees of freedom for the POD-based reduced-order SCNMFE formulation were far fewer than those for classical SCNMFE formulation, so it can greatly lessen the truncation error accumulation in the computational process, alleviate the calculating load, reduce the time required for the calculations, and improve actual computational accuracy. Therefore, after a specific time, the relative deviations (which are computed by means of the formula $[r^k - \sum_{k=1}^N (r^k/N)]/\sum_{k=1}^N (r^k/N)$, $r = \boldsymbol{u}$ or p) of the POD-based reduced-order SCNMFE solutions were fewer than those of the classical SCNMFE solutions (see Figures 10 and 11). Thus, the POD reduced-order SCNMFE solutions are better and more stable than the classical SCNMFE solutions after longer time. Especially, the POD-based reduced-order SCNMFE solutions of pressure are

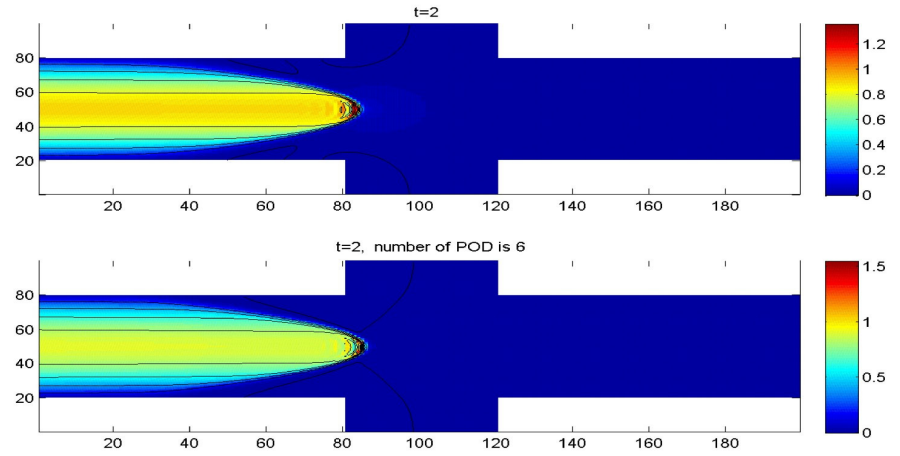

Figure 2. Top chart is the classical SCNMFE solution of velocity $\boldsymbol{u}$ and bottom chart is the POD-based reduced-order SCNMFE solution of velocity $\boldsymbol{u}$ with 6 POD bases when $Re = 1000$ and $Pr = 7$ at time $t = 2$.

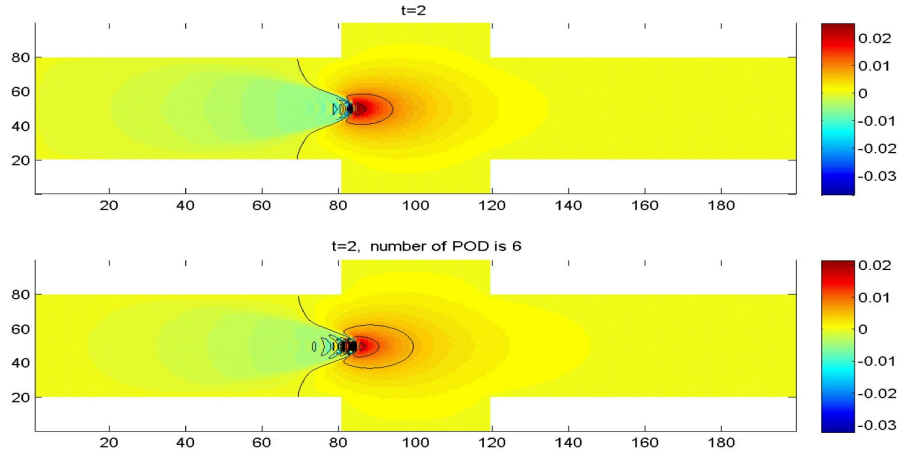

Figure 3. Top chart is the classical SCNMFE solution of pressure p and bottom chart is the POD-based reduced-order SCNMFE solution of pressure p with 6 POD bases when $Re = 1000$ and $Pr = 7$ at time $t = 2$.

obviously better than the classical SCNMFE solutions.

Figure 12 shows the mean absolute errors (MAE) between solutions obtained using the POD-based reduced-order SCNMFE formulation of Problem V with different number of POD bases and solutions obtained using the classical SCNMFE formulation of Problem IV when $t = 5$, $Pr = 7$, and $Re = 1000$. These results show that the numerical results were consistent with the theoretical ones because both were $O(10^{-4})$.

Furthermore, we compared the classical SCNMFE formulation Problem IV with the POD-based reduced-order SCNMFE formulation of Problem V con-

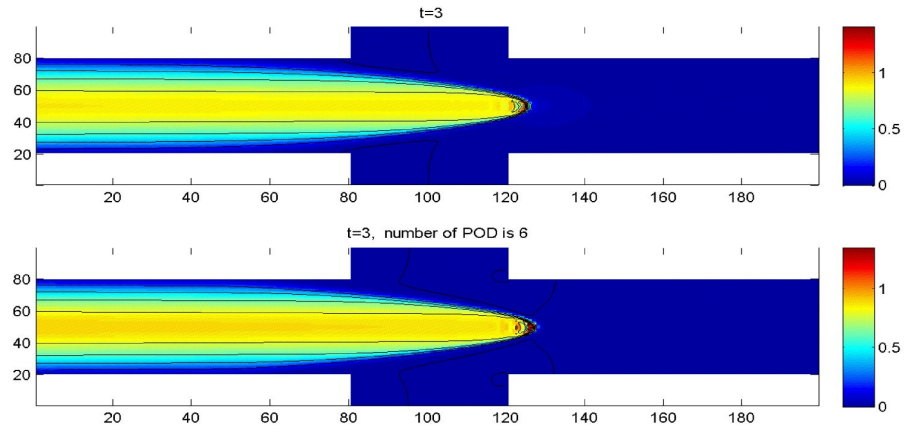

Figure 4. Top chart is the classical SCNMFE solution of velocity $\boldsymbol{u}$ and bottom chart is the POD-based reduced-order SCNMFE solution of velocity $\boldsymbol{u}$ with 6 POD bases when $Re = 1000$ and $Pr = 7$ at time $t = 3$.

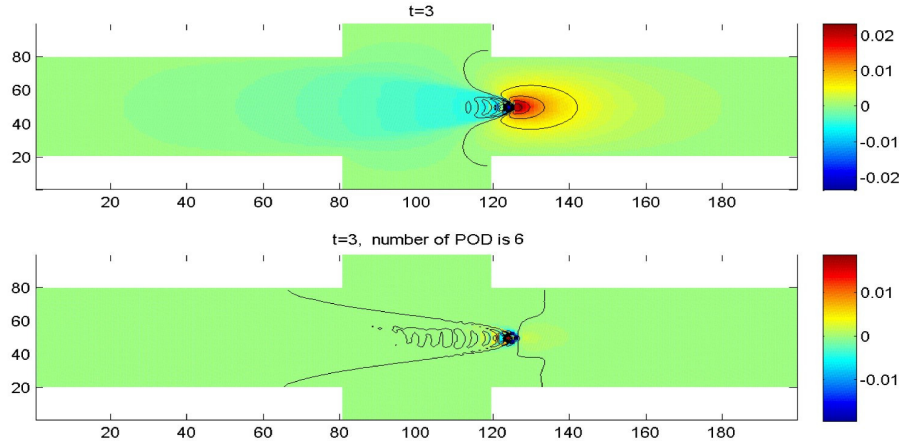

Figure 5. Top chart is the classical SCNMFE solution of pressure p and bottom chart is the POD-based reduced-order SCNMFE solution of pressure p with 6 POD bases when $Re = 1000$ and $Pr = 7$ at time $t = 3$.

taining six POD bases by implementing the numerical simulation computations where $t = 5$, $Pr = 7$, and $Re = 1000$, which shown that the computing time required for the classical SCNMFE formulation Problem IV was 240 minutes, whereas the corresponding computing time for the POD-based reduced-order SCNMFE formulation Problem V with six POD base was only 60 seconds, i.e., the computing time of the classical SCNMFE formulation of Problem IV was 240 times that of the POD-based reduced-order SCNMFE formulation Problem V with 6 POD bases. Thus, we showed that the POD-based reduced-order SCNMFE formulation can greatly save the time-consuming of calculations and

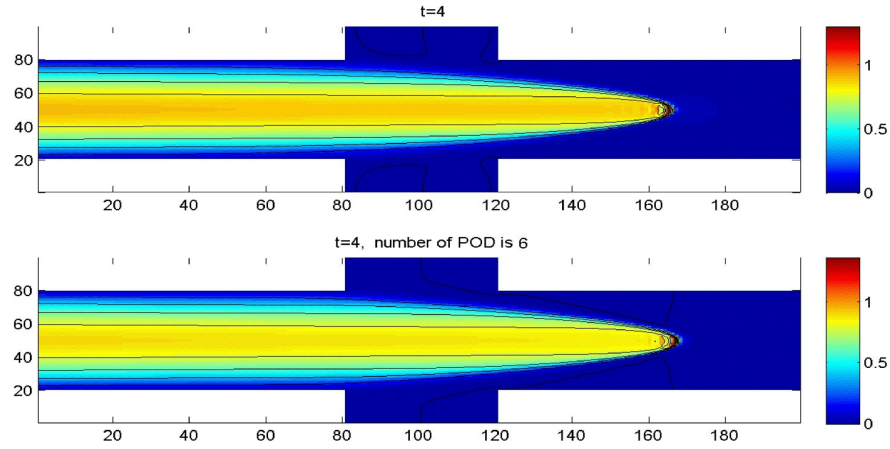

Figure 6. Top chart is the classical SCNMFE solution of velocity $\boldsymbol{u}$ and bottom chart is the POD-based reduced-order SCNMFE solution of velocity $\boldsymbol{u}$ with 6 POD bases when $Re = 1000$ and $Pr = 7$ at time $t = 4$.

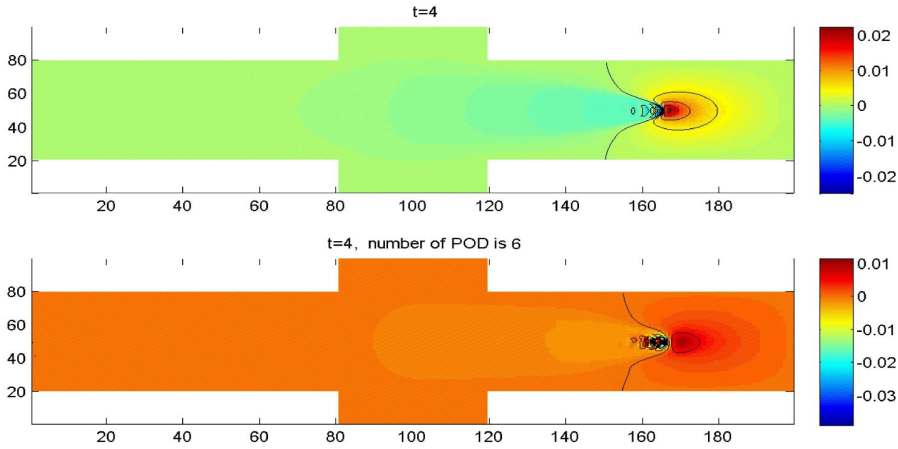

Figure 7. Top chart is the classical SCNMFE solution of pressure p and bottom chart is the POD-based reduced-order SCNMFE solution of pressure p with 6 POD bases when $Re = 1000$ and $Pr = 7$ at time $t = 4$.

alleviate the computational load. We also showed that seeking the numerical solutions for the non-stationary parabolized Navier–Stokes equations using the POD-based reduced-order SCNMFE formulation is computationally highly effective and feasible.

6 Conclusions

In this study, we employed the POD technique and SCNMFE method to establish the POD-based reduced-order SCNMFE formulation for the non-stationary parabolized Navier–Stokes equations. First, we extracted snapshots from the

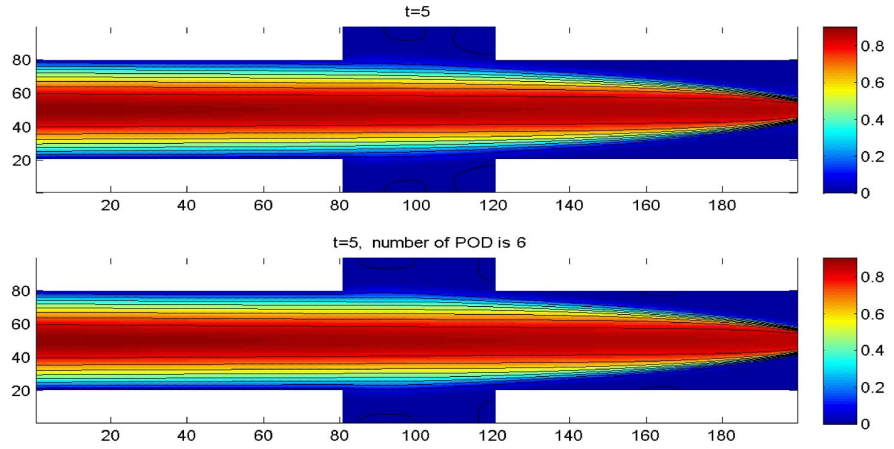

Figure 8. Top chart is the classical SCNMFE solution of velocity $\boldsymbol{u}$ and bottom chart is the POD-based reduced-order SCNMFE solution of velocity $\boldsymbol{u}$ with 6 POD bases when $Re = 1000$ and $Pr = 7$ at time $t = 5$.

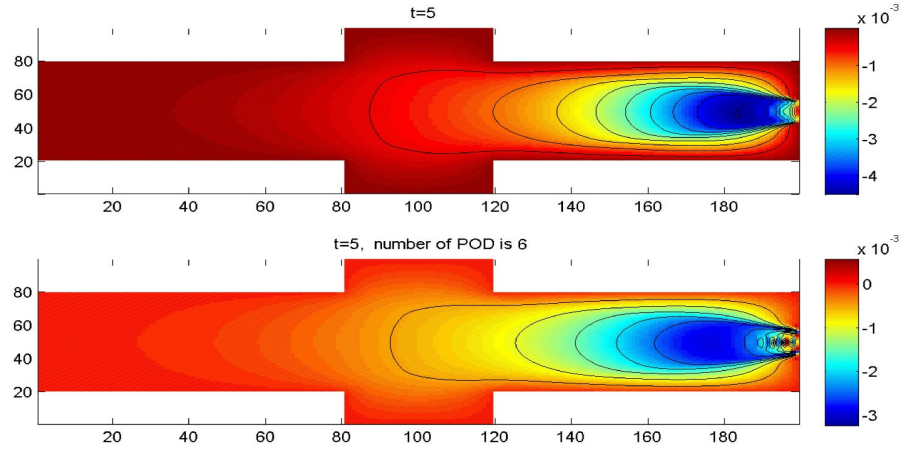

Figure 9. Top chart is the classical SCNMFE solution of pressure p and bottom chart is the POD-based reduced-order SCNMFE solution of pressure p with 6 POD bases when $Re = 1000$ and $Pr = 7$ at time $t = 5$.

first few L ($L \ll N$) numerical solutions to the classical SCNMFE formulation of the non-stationary parabolized Navier–Stokes equations, although in actual applications, we may formulate the snapshots by drawing samples from experiments of physical system trajectories. And then, we formulated the POD basis of the snapshots using the POD method. Next, the FE subspaces of the classical SCNMFE formulation were replaced with the subspaces that spanned a small number of the main POD basis functions, and we established the POD-based reduced-order SCNMFE formulation for the non-stationary parabolized Navier–Stokes equations. Finally, we provided the error estimates between

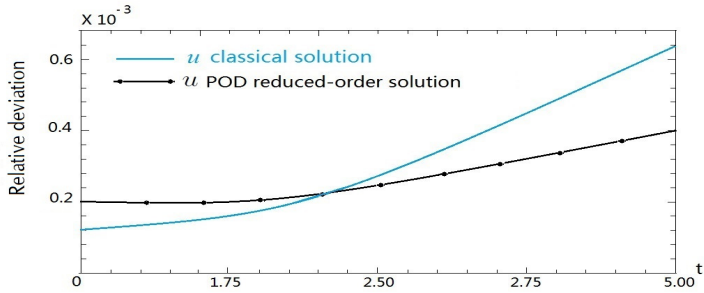

Figure 10. The relative deviations of the classical SCNMFE solution and the POD-based reduced-order SCNMFE solution with 6 POD bases of velocity $\boldsymbol{u}$ for $Re = 1000$ on $0 \leqslant t \leqslant 5$.

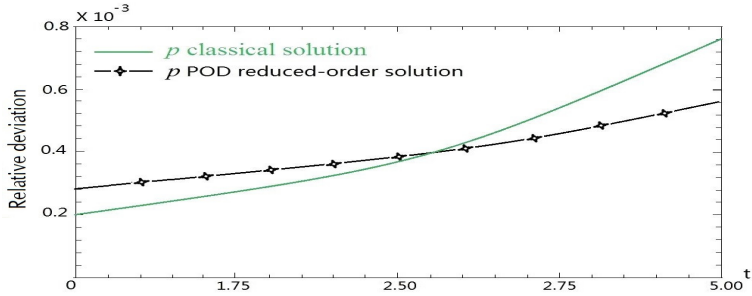

Figure 11. The relative deviations of the classical SCNMFE solution and the POD-based reduced-order SCNMFE solution with 6 POD bases of pressure p for $Re = 1000$ on $0 \leqslant t \leqslant 5$.

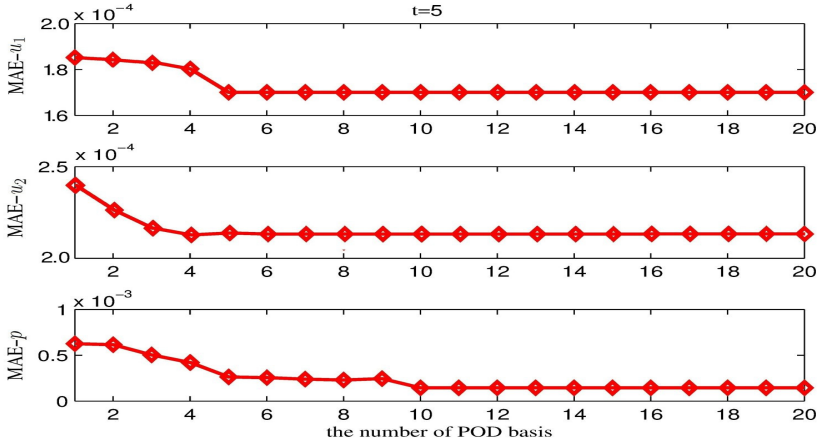

Figure 12. Absolute error for $Re = 1000$ and $Pr = 7$ when POD basic is different and at the time level $t = 5$.

the classical SCNMFE solutions and the POD-based reduced-order SCNMFE formulation solutions and the algorithm implementation for solving the POD-based reduced-order SCNMFE formulation of the non-stationary parabolized Navier–Stokes equations. Moreover, some numerical experiments had verified that the numerical results were consistent with the theoretical ones, thus validating both the feasibility and efficiency of the POD-based reduced-order SCNMFE formulation.

Acknowledgements
Author would like to acknowledge cordially four anonymous referees and editors for their valuable comments which lead to the improvement of this paper.

References

[1] R.A. Adams. *Sobolev Spaces*. Academic Press, New York, 1975.

[2] A.K. Alekseev, I.M. Navon and J.L. Steward. Comparison of advanced large–scale minimization algorithms for the solution of inverse ill-posed problems. *Optim. Methods Soft.*, **24**(1):63–87, 2009. http://dx.doi.org/10.1080/10556780802370746.

[3] J. An, P. Sun, Z.D. Luo and X.M. Huang. A stabilized fully discrete finite volume element formulation for non-stationary Stokes equations. *Math. Numer. Sin.*, **33**(2):213–224, 2011.

[4] Y. Bourgault, P. Caussignac and L. Renggli. Finite element methods for parabolized Navier–Stokes equations. *Comput. Methods Appl. Mech. Eng.*, **111**(3–4):265–282, 2004.

[5] P.G. Ciarlet. *The Finite Element Method for Elliptic Problems*. North-Holland, Amsterdam, 1978.

[6] D. D'Ambrosio and R. Marsilio. A numerical method for solving the three-dimensional parabolized Navier–Stokes equations. *Comput. Fl.*, **26**(6):587–611, 1997. http://dx.doi.org/10.1016/S0045-7930(97)00007-8.

[7] J. Du, I.M. Navon, J.L. Steward, A.K. Alekseev and Z.D. Luo. Reduced order modeling based on POD of a parabolized Navier–Stokes equations model I: Forward model. *Int. J. Numer. Methods Fl.*, **69**(3):710–730, 2012. http://dx.doi.org/10.1002/fld.2606.

[8] J.G. Heywood and R. Rannacher. Finite element approximation of the non-stationary Navier–Stokes problem, I. Regularity of solutions and second order estimates for spatial discretization. *SIAM J. Numer. Anal.*, **19**(2):275–311, 1982. http://dx.doi.org/10.1137/0719018.

[9] M. Hinze and M. Kunkel. Residual based sampling in pod model order reduction of drift-diffusion equations in parametrized electrical networks. *J. Appl. Math. Mech.*, **92**(2):91–104, 2012.

[10] A. Janon, M. Nodet and C. Prieur. Certified reduced-basis solutions of viscous Burgers equation parametrized by initial and boundary values. *ESAIM: Math. Model. Numer. Anal.*, **47**(2):317–348, 2013. http://dx.doi.org/10.1051/m2an/2012029.

[11] I.T. Jolliffe. *Principal Component Analysis*. Springer-Verlag, Berlin, 2002.

[12] K. Kunisch and S. Volkwein. Galerkin proper orthogonal decomposition methods for a general equation in fluid dynamics. *SIAM J. Numer. Anal.*, **40**(2):492–515, 2002. http://dx.doi.org/10.1137/S0036142900382612.

[13] S. Li and Y. Hou. A fully discrete stabilized finite element method for the time-dependent Navier–Stokes equations. *Appl. Math. Comput.*, **215**(1):58–99, 2009.

[14] Z.D. Luo. *The Foundations and Applications of Mixed Finite Element Methods.* Science Press, Beijing, 2006. (in Chinese)

[15] Z.D. Luo, J. Chen, I.M. Navon and X. Yang. Mixed finite element formulation and error estimates based on proper orthogonal decomposition for the non-stationary Navier–Stokes equations. *SIAM J. Numer. Anal.*, **47**(1):1–19, 2008. http://dx.doi.org/10.1137/070689498.

[16] Z.D. Luo, J. Du, Z.H. Xie and Y. Guo. A reduced stabilized mixed finite element formulation based on proper orthogonal decomposition for the non-stationary Navier–Stokes equations. *Int. J. Numer. Methods Eng.*, **88**(1):31–46, 2011. http://dx.doi.org/10.1002/nme.3161.

[17] Z.D. Luo, H. Li, P. Sun and J.Q. Gao. A reduced-order finite difference extrapolation algorithm based on pod technique for the non-stationary Navier–Stokes equations. *Appl. math. Model.*, **37**(7):5464–5473, 2013. http://dx.doi.org/10.1016/j.apm.2012.10.051.

[18] Z.D. Luo, R.W. Wang and J. Zhu. Finite difference scheme based on proper orthogonal decomposition for the non-stationary Navier–Stokes equations. *Sci. China, Ser. A: Math.*, **50**(8):1186–1196, 2007.

[19] N.C. Nguyen, G. Rozza and A.T. Patera. Reduced basis approximation and a posteriori error estimation for the time-dependent viscous Burgers equation. *Calcolo*, **46**(3):157–185, 2009. http://dx.doi.org/10.1007/s10092-009-0005-x.

[20] V.S. Pratap and D.B. Spalding. Fluid flow and heat transfer in three-dimensional duct flows. *Int. J. Heat Mass Transfer*, **19**:1183–1188, 1976. http://dx.doi.org/10.1016/0017-9310(76)90152-6.

[21] D.V. Rovas, L. Machiels and Y. Maday. Reduced-basic output bound methods for parabolic problems. *IMA J. Numer. Analy.*, **26**:423–445, 2006. http://dx.doi.org/10.1093/imanum/dri044.

[22] W. Rudin. *Functional and Analysis (2nd ed.).* McGraw-Hill Companies Inc., 1973.

[23] R. Temam. *Navier–Stokes Equations (3rd ed.).* North-Holland, Amsterdam, New York, 1984.

[24] K. Veroy and A.T. Patera. Certified real-time solution of the parametrized steady incompressible Navier–Stokes equations: Rigorous reduced-basis a posteriori error bounds. *Int. J. Numer. Methods Fl.*, **47**(8–9):773–788, 2005. http://dx.doi.org/10.1002/fld.867.

[25] K. Veroy, C. Prud'homme and A.T. Patera. Reduced-basis approximation of the viscous burgers equation: rigorous a posteriori error bounds. *Compt. Rend. Math.*, **37**(9):619–624, 2003. http://dx.doi.org/10.1016/j.crma.2003.09.023.

[26] R. Wang and Y. Shen. Numerical solutions of the diffusion parabolized Navier–Stokes equations. *Adv. Mech.*, **35**(4):481–497, 2005.

[27] Y.J. Zhou, F. Teng and Z.D. Luo. A stabilized Crank–Nicolson mixed finite element method for the non-stationary parabolized Navier–Stokes equations. *Acta Math. Appl. Sin.*, 2014. in press (Accepted for Publication)